Journal of Achievements in Materials and Manufacturing Engineering
VOLUME 31
ISSUE 2
December
2008

Surface integrity on hardened steel parts produced by hybrid machining sequences

W. Grzesik [a], J. Rech [b,*], T. Wanat [a]
[a] Department of Manufacturing Engineering and Production Automation, Opole University of Technology, Poland
[b] Laboratory of Tribology and Systems Dynamics, ENISE, Saint-Etienne, France
* Corresponding author: joel.rech@enise.fr

Received 05.09.2008; published in revised form 01.12.2008

Manufacturing and processing

ABSTRACT

Purpose: Of this paper is the investigation of surface integrity generated in hard turning and subsequent finish abrasive machining. The primary reason for undertaking this problem was insufficient magnitude of compressive residual stresses after hard turning which determines the fatigue resistance of highly loaded transmission parts.
Design/methodology/approach: Employed uses 2D and 3D description of the surface roughness/surface microstreometry and the X-ray diffraction method for measurements of residual stresses. The main scope of this research program is to record the relevant changes of surface layer features resulting from the application of finish abrasive passes.
Findings: Can be distinguished into two groups. First, finish belt grinding produces the residual stresses with the maximum value of–1000 MPa, which is satisfactory for improving fatigue life. Second, the bearing properties improve due to displaying negative values of the skew.
Research limitations/implications: Deal with the identification range of 3D roughness parameters and the lack of modern equipment for robust measurements of residual stresses: Future research should be focused on the stronger correlation between technological and exploitation properties of the surfaces produced by hard and abrasive technologies. However, it needs more detailed inputs from automotive industry.
Practical implications: Are related to the automotive industry, especially to manufactures of such transmission elements as synchronizing cones/planes on gear wheels. The sequences of new hybrid machining processes are partly verified in terms of industry needs (machining conditions, machine tools, special equipment, cutting and abrasive tools).
Originality/value: Of this industry–oriented contribution is based on the aggregating hard cutting and abrasive machining processes. The practical value of the paper is that it proposes a very beneficial machining process for highly loaded hardened parts.
Keywords: Machining; Hybrid process; Surface roughness; Residual stress

1. Introduction

To replace conventional grinding of hardened steel components, precision finishing with superhard cutting tools can be offered to manufacturers as an attractive alternative. This is because it can allow cutting manufacturing costs, decreasing production time, and improving overall product quality [12, 23]. Hard turning (HT) is usually performed on steel workpieces harder than 60 HRC with both mixed ceramic and PCBN cutting tools. It can be extended to rough, precision, and high precision operation when the Rz parameter is less than 1 μm [12].

Industry feedback indicates that hard machining (HM), known as hard part machining (HPM), includes both semi-finishing and finishing turning as well as milling operations. Turned parts are typically gears, axles and bearing components, whereas milling is predominantly used in the die and mold industry [23].

It was previously revealed that HT finishing operations with mixed ceramic and low content CBN (CBN-L) tools result in surface finish with the Ra roughness parameter about 0.2÷0.3 or Rz parameter of 1÷2 μm [3, 14, 15, 17, 20]. As the first, Klocke et al. and Grzesik and Wanat [5, 6, 12] established multi-parameter 2D and 3D characterization of the surface finish produced by hard turning. One of the basic innovations of these investigations is that hard turning and grinding processes provide surface profiles with different forms and surfaces with dissimilar topography structures. In particular, hard turning generates surface profiles with negative skewness (Rsk < 0), which denotes better bearing properties.

It is apparent that HT technology produces the surface integrity which is often not sufficient for high performance parts with strong demands concerning fatigue life or pitting resistance. As a result, hard turning leads to the following service limitations, namely [1, 9, 12, 13, 19, 21, 22] compressive residual stresses of low magnitudes, the process-induced white layer leading to unpredictable variations in service performance of such components, dimensional and geometrical form errors, and surface roughness deterioration resulting from excessive tool wear.

Commonly, appropriate surface quality and fatigue strength of gears, bearing rings, crankshafts, camshafts, etc. is usually provided by grinding-based technology, i.e. microfinishing, superfinishing or honing. It was found that hard turning requires further abrasive finishing processes such as CBN grinding and belt grinding when applying to synchronizing cones/planes on gearwheels [19, 20, 24]. It is reported [10, 19] that finishing belt grinding induces higher compressive tangential residual stresses, a few microns beneath the outer surface. This enables partial or entire removal of the white layer.

The results provided by Abrão and Aspiwall [1] indicated that compressive residual stresses were induced in the hardened AISI E52100 (62 ±1 HRC) after hard turning with CBN and ceramic tools, and the depth of their highest values of -600 MPa was approximately 5÷20 μm surface. On the other hand, after classical grinding the highest stress value was measured on the workpiece surface. The role of residual compressive stresses can be beneficial in improving fatigue performance of workpieces with surfaces of > 0.1 μm Ra [16, 18]. As concluded in [18], in the absence of residual stress, machined surface roughness values in excess of 0.1 μm Ra have a strong influence on fatigue life.

As yet, surface finish produced by hybrid processes have not been explored. There was an impulse to thoroughly investigate surface finish on the parts from hardened bearing steel when abrasive operations follow single-point hard turning.

2. Experimental program

2.1. Machine tools and machining conditions

In this research, a specially designed, ultra-precision facing lathe was used to carry out CBN turning operations. This special design concerns such elements as granite body, the thermally controlled spindle, direct tool clamping on the table, and the chuck and jaws with improved rigidity and accuracy.

A CNC lathe with Siemens 840D control system was employed to achieve the displacements less than 0.1 μm. In a part of hard turning tests (HT1 in Table 1) the triangular inserts with 60% CBN content were selected. The cutting edges were prepared with a chamfer of 0.1 mm wide, –20º inclination angle, and the honing radius of 0.05 mm. Cutting speed v_c = 100 m/min, feed rate f = 0.1 mm/rev, and depth of cut a_p = 0.3 mm were used. On the other hand, hard turning operations with mixed ceramic tools (HT2) were performed on a precision lathe. Consequently, cutting speed v_c = 115 m/min, feed f = 0.1 mm/rev, and depth of cut a_p = 0.3 mm were selected.

New technique of belt grinding was used, as mentioned in the introduction. As a result, belt grinding operations were performed on a special device mounted on the lathe, shown in Fig 1. The abrasive belt consisted of a single layer of Al_2O_3 abrasive grains which was stocked on an elastic paper strip reinforced with fibres. Nearly homogenous pressure of 2 bars between the workpiece and the belt was exerted by means of a polymer roller of 70º Sh (Shore) hardness, denoted by “5” in Fig. 1. At the microscopic scale, the contact is localized within the peaks of abrasive grains. The pressures developed in the local contact zones are high enough to perform material removal and to generate compressive residual stresses resulting from the strain-hardening effect. The process duration was less than 10 s to confirm the expectations of real industrial applications. The cooling was a MQL system (trade mark-ARLAMATIC) with two nozzles orientated along the contact line.

The first operation sequence includes belt grinding operations with 30μm (BG1) and 9 μm (BG2) grains performed after PCBN turning (HT1) on the device show in Fig. 1 during 9 sec under MQL conditions [19]. The following process conditions were used: rotation speed of the workpiece of 900 rev/min, belt feed of 0.6 mm/s, defined pressure of 2 bars between the workpiece and the belt, axial oscillation of 12 Hz frequency and 1 (±0.5) mm in amplitude.

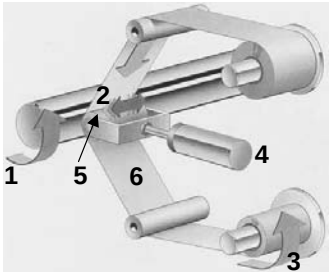

Fig. 1. Kinematical scheme of belt grinding process: 1 – work rotation, 2 – belt oscillation, 3 – belt reeling, 4 – pressure regulation, 5 – pressure roller, 6 – grinding belt

In the second variant, the turned surfaces (HT2) were abrasively finished with 29 μm grain stones using intensive mist cooling and other process conditions specified in Table 1.

2.2. Measurements of surface roughness

In this study the measurements of 2D and 3D roughness parameters were carried out by means of a TOPO 01P and Hommel-Somicronic profilometers [7, 10, 19]. Accordingly, SURFSCAN and TOPOSURF programs were applied to analyze 2D surface profiles and 3D surface texture. The scanned areas of 4×4 mm and 1.25×1.25 mm were selected when using a TOPO 01P profilograph. Cut-off length was set, depending on the type of machining operation, to 0.8 mm (the evaluation length was equal to l_n = 4.8 mm) and 0.25 mm (corresponding l_n = 1.5 mm) according to ISO 4288, and the ISO 2CR filter was selected. In summary, selected height (Ra, Rz, Rp, Rv, Sa, Sz, Sp, Sv), spacing (RSm), angle (RΔq) and profile height distribution (Rsk, Rku, Rmr(c)) were measured. Correspondingly, in order to reflect the specific properties of the surfaces generated, amplitude distribution functions (ADFs), bearing area curves (BACs), surface topographies, and contour maps for the four surface types selected were determined.

2.3. Measurements of residual stresses

In this study the biaxial residual stress with tangential (σ_{11}) and axial (σ_{22}) components (Fig. 2) was measured using the X-ray diffraction method. The measurements were performed using a Philips X'Pert MRD system with a horizontal, high-resolution Ω-2Θ goniometer (PW3050/20 HR) [4, 25].

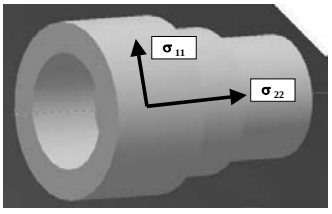

Fig. 2. Scheme of residual stress resolution in the specimen

This apparatus was operated at 40 kV tension, 40 mA current (1.8 kW) using CrKα radiation (λ = 2.2897Å) and Bragg-Bretano configuration. The Ψ tilts were achieved with omega-goniometry, tilting in the diffraction plane. The measurements were carried out in the (211) martensite peak, localized at 2Θ = 156º, at 39 different orientations. Residual stresses were measured at the surface and at different depths by successive etching ultra-thin stressed layers up to 200 μm. The RIM (X-ray Integral Method) was used to calculate residual stress depth profiles with accuracy of ±60 MPa [4].

3. Experimental results and discussion

3.1. Height and spacing roughness parameters

This section surveys the changes of the SRa, SRz, SRp, SRv, Rsm and RΔq roughness parameters, produced by single hard turning operations and three sequences of finishing abrasive processes. They are successively presented in Figs. 3÷5.

Fig. 3 shows that the two hard turning operations (bars 1 and 3) yield surfaces with average values of SRa (Ra) parameters about 0.35(0.3) and 0.45(0.4) μm respectively. Furthermore, belt grinding (2) and honing (4) operations allow decreasing their values to 0.02 (0.02) and 0.35(0.3) μm, respectively.

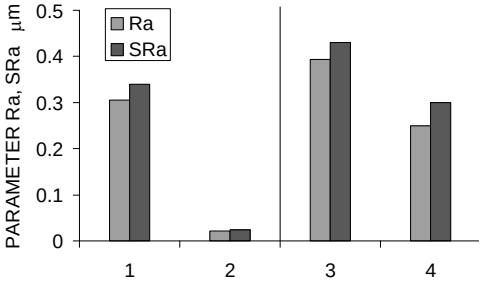

Fig. 3. Comparison of Ra and SRa parameters for HT1 (1), HT1+BG1, 2 (2), HT2 (3) and HT2+SF (4) operations

Table 1.
Specification of operations and machining conditions

	Symbol	Type of machining process	Process conditions
1	HT1	CBN hard turning	TNGA160408S01020-7020 Sandvik's insert v_c = 100 m/min, f = 0.1 mm/rev, a_p = 0.3 mm
2	HT2	Hard turning with mixed ceramic (MC) tools	SNGN120408T01020-CC650 Sandvik's insert (71% Al_2O_3, 28% TiC and 1% others) v_c = 115 m/min, f = 0.1 mm/rev, a_p = 0.3 mm
3	HT1+BG1	CBN hard turning plus belt grinding with 30μm grains	Rotation speed of the workpiece 900 rev/min, belt feed 0.6 mm/s, oscillation frequency 12Hz, oscillation magnitude +/- 0.5 mm, pressure 2 bars, belt grinding duration 9 sec, cooling system: MQL
4	HT1+BG(1,2)	CBN hard turning plus two belt grinding operations with 30μm (BG1) and 9 μm grains (BG2)	
5	HT2+SF	MC hard turning with plus superfinishing	Honing stone reference 99A320N10V oscillation frequency 680 osc/min, applied force 40N, amplitude 3.5 mm; size of grains 29μm, cooling medium 85% kerosene and 15% machine oil

Fig. 4 shows the SRz (SL peak to valley height) and its two components SRp (maximum peak height) and SRv (maximum valley height). It is evident from Fig. 4 that the partition of SRp and SRv components within the total profile height vary substantially depending on the process sequence implemented.

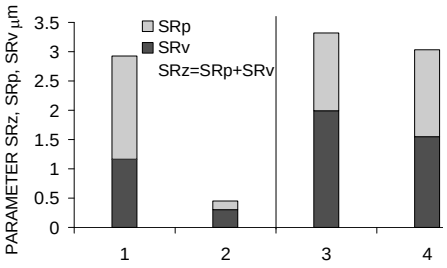

Fig. 4. Participation of peaks and valleys in profiles for HT1 (1), HT1+BG1,2 (2), HT2 (3) and HT2+SF (4) operations

For instance, profiles resulting from HT2 operations (3) contain lower peaks and deeper valleys. In contrast profiles obtained in PCBN turning (HT1) are dominated by higher peaks and lower valleys. Particulary, the process containing 9 µm belt grinding causes the ratio of SRp (0.15 µm) to SRv (0.30 µm) to decrease down to 0.5, whereas after preliminary turning it is about 1.5. Finally, the SRz parameter decreases to 0.3 µm (parallely the value of SRp/SRv increases from 0.7 to about 1) after honing (4).

As can be seen from Fig. 5, the average spacing RSm decreases considerably after belt grinding passes, from 62.5 µm down to 20.5 µm when using belt with finer grains. On the contrary, the peak spacing produced by HT with ceramic tools was reduced about 20% (79.5 µm vs. 62.5 µm) through honing operations. In addition, RMS slope of irregularities RΔq decreases and oscillates slightly about 4º after both finish abrasive processes.

a) RSm = 62.5 µm, RΔq = 5.6º

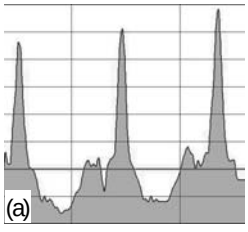

b) RSm=20.5 µm, RΔq = 3.9º

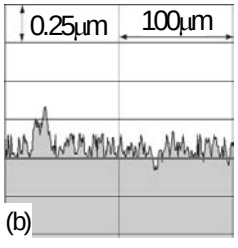

Fig. 5. Characteristic shapes of 2D profiles for HT1 (a) and HT1+BG1,2 (b) operations

3.2. Visualization of surfaces

Figs 6÷10 show some selected topographies of the scanned machined surfaces. Appropriate 3D roughness parameters were the same as listed in Section 3.1.

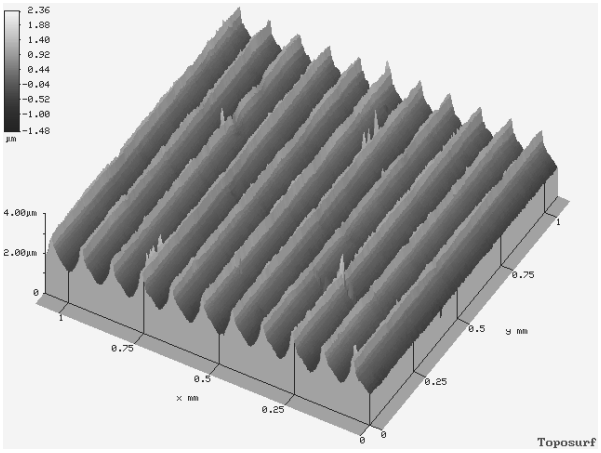

Fig. 6. Isometric view of surface machined with CBN tools HT1, Sra = 0.35µm

By analogy to the surface profiles shown in Fig. 5, corresponding topographies produced by CBN tools (Fig. 6) include visible regular sharp peaks. In contrast, the modified surfaces presented in Figs 7 and 8 contain randomly distributed irregularities with progressively smaller height of SRz = 2.53 µm and 0.45µm, respectively.

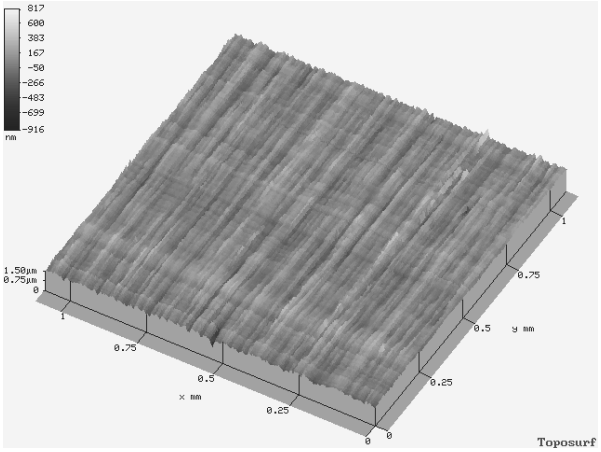

Fig. 7. Isometric view of surface after CBN turning and finish belt grinding (HT1+BG1), Sra = 0.12 µm

Similar effects to the belt grinding with 30 µm grains can be obtained after superfinishing of previously turned surfaces, as illustrated in Figs 9 and 10. In this hybrid machining sequence the SRz parameter was reduced from 3.3 µm to about 3 µm.

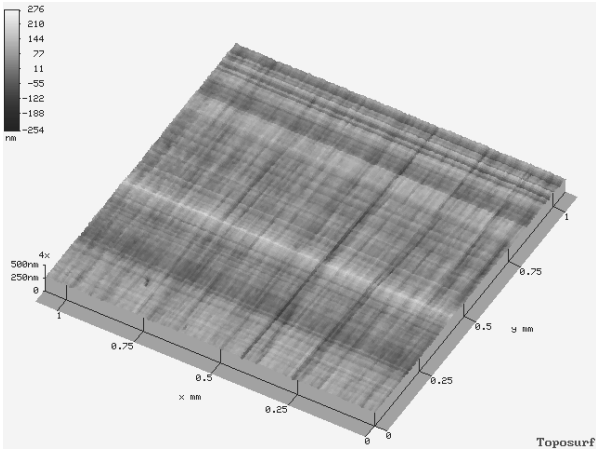

Fig. 8. Isometric view of surface after CBN turning and finish belt grinding (HT1+BG1,2), Sra = 0.02 μm

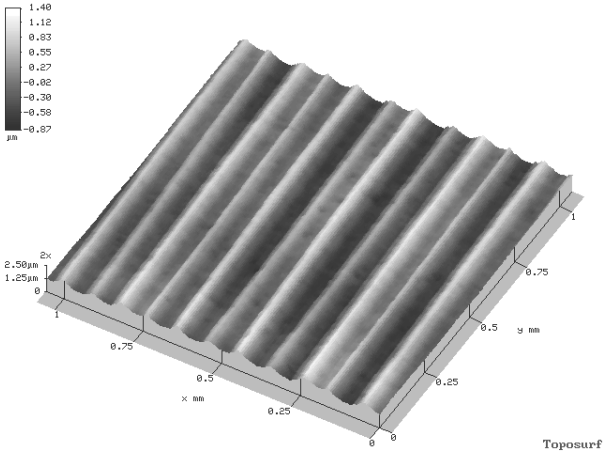

Fig. 9. Isometric view of surface machined with mixed ceramic tools (HT2), Sra = 0.43 μm

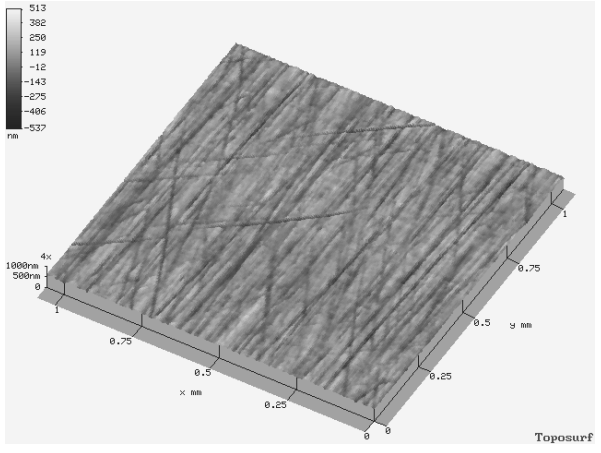

Fig. 10. Isometric view of surface machined with ceramic tools and abrasive stones (HT2+SF), Sra = 0.30μm

The regularity of the feed marks characteristic for both single-point CBN and MC tools, shown in Figs 6 and 9, is confirmed in the contour maps presented in Figs 11 and 12. The topographies of surfaces after MC turning (Fig. 9) and subsequent superfinishing (Fig. 10) were generated by the scanning technique using a TOPO 01P profilograph.

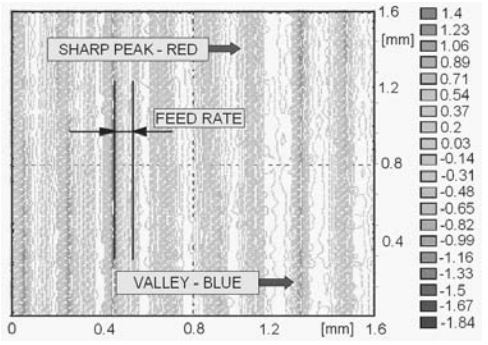

Fig. 11. Contour map for surface turned with ceramic tool and feed rate f = 0.1 mm/rev

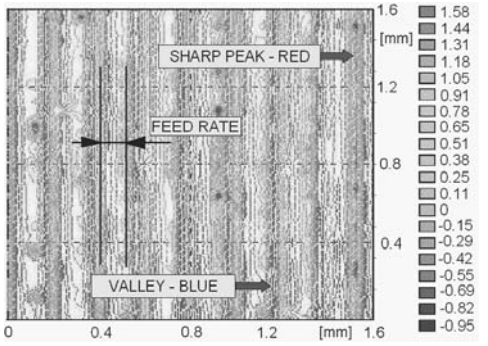

Fig. 12. Contour map for surface turned with CBN tool and feed rate f = 0.1 mm/rev

Narrow bands placed at the distance equal to the feed rate are represented by appropriate red or green sharp summits. Additionally, some local micro-peaks on individual irregularities can be recognized in Fig. 12. On the other hand, the random distribution of peaks for the surface after belt grinding is observed in Fig. 13.

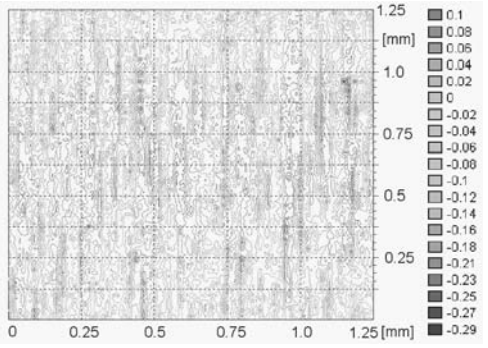

Fig. 13. Contour map for surface turned with CBN tool as in Fig. 12 and belt ground (HT1+BG(1,2))

3.3. Profile height distribution parameters

Fig. 14 shows the subsequent changes recorded for the bearing curves. In general, the BACs have characteristic degressive-progressive shapes. In particular, after belt grinding the identical values of Rmr(20) parameter correspond with depths c = 62% (2) and 70% (3), but for CBN turning this value is observed for c = 38% (1). Similar tendency, i.e. the cut *c* increases from 54% (4) to 64% (5) is documented after honing. It should also be noted that all finishing abrasive processes produce negative values of skew (about -0.2 for BG and -0.5 for SF), which can improve bearing properties of the machined surfaces.

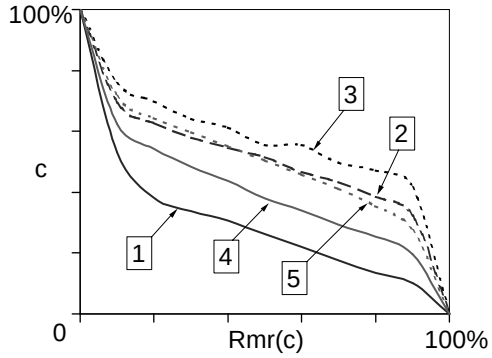

Fig. 14. Differences in BACs curves obtained in cutting and finish abrasive operations. 1 – HT1, 2 – HT1+BG1, 3 – HT1+BG1,2, 4 – HT2, 5 – HT2+SF

Fig. 15 shows the plot kurtosis Rku versus skewness Rsk. It is evident that finishing abrasive processes allow obtaining negative values of skew (about -0.2 for belt grinding and -0.5 for honing), which improve bearing properties of the surfaces.

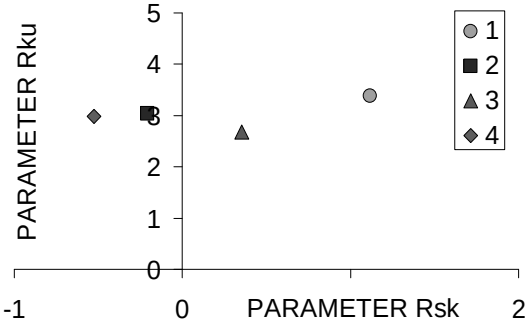

Fig. 15. Skew *vs.* kurtosis for HT1 (1), HT1+BG1,2 (2), HT2 (3) and HT2+SF (4) operations

Correspondingly, Fig. 16 illustrates the transformation of the FDA curves obtained for profiles generated by PCBN turning and subsequent two belt grinding passes. In order to compare these individual effects, an ideal Gaussian curve (G) corresponding to the value of Rku = 3 was added.

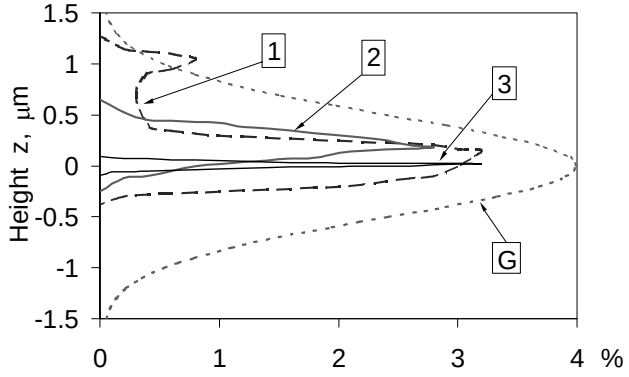

Fig. 16. Transformation of FDA curve for PcBN after belt grinding. 1 – HT1, 2 – HT1+BG1, 3 – HT1+BG1,2, G – ideal Gaussian profile (Rsk = 0, Rku = 3)

3.4. Capability of contact load

Figs 17 and 18 present the SCGCs (Symmetrical Curves of Geometrical Contact) constructed as mirror images of the relevant bearing curves [11], for two hybrid technological chains with different mechanisms of the generation of final surface texture. As reported in [5, 6], the SCGC defines the boundaries of working area within the surface profile, correlating to the bearing and contact load capacity, the desired lubricant volume and the material volume predicted for removing by abrasive wear.

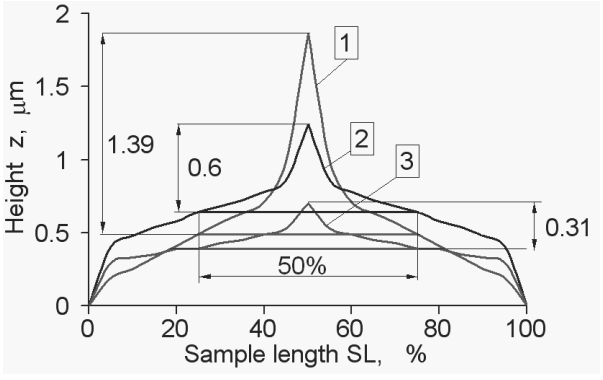

Fig. 17. SCGC curves for surfaces after CBN turning (1) and belt grinding with 30 µm (2) and 9 µm (3) grains

As can be seen in Figs 17 and 18, one can control the position of the defined material ratio level. For example, for the combination of CBN turning with two-pass belt grinding the position of the line corresponding to the material ratio Rmr50% is gradually reduced from 1.39 µm, through 0.6 µm (BG1) down to 0.31 µm (BG2). Correspondingly, after MC turning and superfinishing the Rmr50% decreases from 1.29 µm to 0.51 µm. This fact coincides well with the relevant shapes of bearing curves (2) and (5) in Fig. 14.

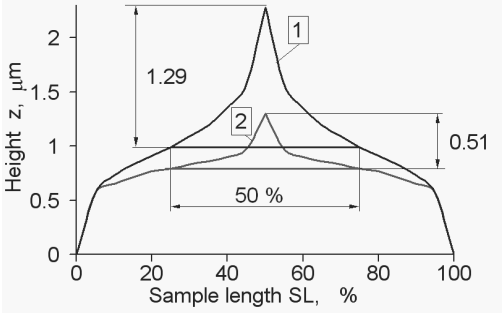

Fig. 18. SCGC curves for surfaces after MC turning (1) and external honing (2)

3.5. Residual stress distribution

Distribution profiles of the tangential and axial stress components determining in the CBN turned and belt ground surfaces are shown in Fig. 19 a and b, respectively.

Fig. 19 presents two exemplary distributions of the residual stresses for each component determined by means of the X-ray diffractometry. It is clear from Fig. 19 that although the peaks with tensile stresses are localized at the depth of a few microns beneath the surface, the compressive residual stresses are measured at the belt ground surfaces, similar to case-hardened steel [19].

a)

b)

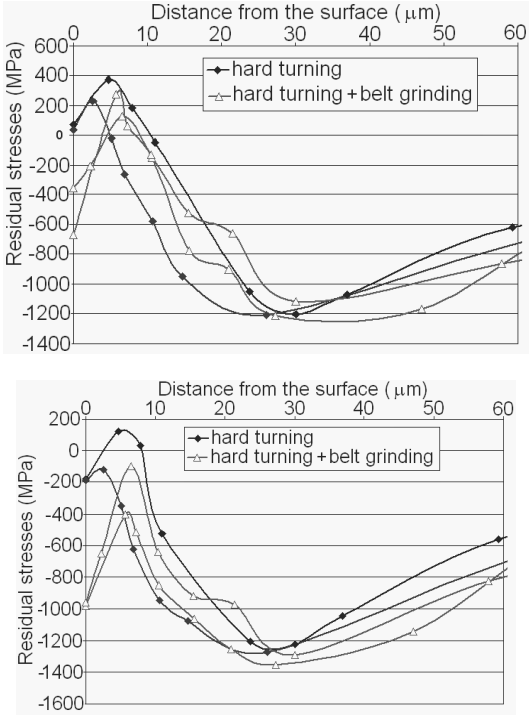

Fig. 19. Distributions of residual stresses in the sublayer obtained after CBN hard turning and belt grinding operations: a) tangential σ_{11} and b) axial σ_{22} stresses

Comparison of stress distributions illustrated in Fig. 19a and b reveals that axial residual stresses are higher than tangential ones and reached the values of about -1000 MPa. The highest compressive stresses in the magnitude of (-1200)÷(-1400) MPa were measured in depth of about 30 µm. It should also be noted that hard turning induced tensile tangential and axial stresses of 150÷400 MPa at a small distance from the surface.

4. Summary

Finish abrasive passes result in changing both height and spacing roughness parameters. The relevant ratios of SRp to SRv for belt grinding and superfinishing were found to be 0.5 and 1.

It is noted that an elastic belt influences both valleys and peaks of the surface, whereas a rigid abrasive stone modifies the shape of the peaks above the CLA.

One can control the position of the defined material ratio level by performing finish abrasives [8]. For example, for the combination of CBN turning with belt grinding the position of the line corresponding to the material ratio Rmr50% is gradually reduced by as much as four times.

Hard turned surfaces, treated additionally by abrasives, display negative values of the skew. It suggests better bearing properties in comparison to simple hard turning passes. This effect is basically observed for PCBN turning and following belt grinding.

Compressive residual stresses occurring at the machined surface were determined after belt grinding. In comparison, CBN hard turning induced tensile stresses localized at the distance of a few microns beneath the machined surface. In general, the 9 µm belt grinding leads to the localization of residual stresses in a very thin sublayer of ~5 µm.

References

[1] A.M. Abrão, D.K. Aspinwall, The surface integrity of turned and ground hardened bearing steel, Wear 196 (1996) 279-284.

[2] G.C. Benga, A.M. Abrão, Turning of hardened 100Cr6 bearing steel with ceramic and PCBN cutting tools, Journal of Materials Processing Technology 143-144 (2003) 237-241.

[3] Y.K. Chou, Ch.J. Evans, M.M. Barash, Experimental investigation on CBN turning of hardened AISI 52100 steel, Journal of Materials Processing Technology 124 (2002) 274-283.

[4] C. Garcia-Rosales, X-ray diffraction measurements and data analysis, personal communication, CEIT&TECNUN, Universidad de Navarra, San Sebastian, Spain, 2006.

[5] W. Grzesik, T. Wanat, Comparative assessment of surface roughness produced by hard machining with mixed ceramic tools including 2D and 3D analysis, Journal of Materials Processing Technology 169 (2005) 364-371.

[6] W. Grzesik, T. Wanat, Surface finish generated in hard turning of quenched alloy steel parts using conventional and wiper ceramic inserts, International Journal of Machine Tools and Manufacture 46/15 (2006) 1988-1995.

[7] W. Grzesik, S. Brol, Hybrid approach to surface roughness evaluation in multistage machining processes, Journal of Materials Processing Technology 134 (2003) 265-272.
[8] W. Grzesik, J. Rech, T. Wanat, Surface integrity of hardened steel parts in hybrid machining operations, Journal of Achievements in Materials and Manufacturing Engineering 18 (2006) 367-370.
[9] Y.B. Guo, J. Sahni, A comparative study of hard turned and cylindrically ground white layers, International Journal of Machine Tools and Manufacture,44 (2004) 135-145.
[10] A. Jourani, M. Dursapt, H. Hamdi, J. Rech, H. Zahouani, Effect of the belt grinding on the surface texture: modeling of the contact and abrasive wear, Wear 259 (2005) 1137-1143.
[11] J. Kaczmarek, E. Kulawik, New approach to the characteristics of surface microstereometry on the basis of facing, Advances in Technology Machines and Equipment 23 (1999) 55-70.
[12] F. Klocke, E. Brinksmeier, K. Weinert, Capability profile of hard cutting and grinding processes, CIRP Annals 54 (2005) (in press).
[13] W. König, M. Klinger, R. Link, Machining hard materials with geometrically defined cutting edges-field of applications and limitations, CIRP Annals 39 (1990) 61-64.
[14] J. Kundrak, V. Bana, K. Gyani, 3D Topography of hard turned and ground surfaces, Proceedings of the 3rd International Congress of Precision Machining ICPM'2005, Vienna, 2005, 195-202.
[15] J.G. Lima, R.F. Ávila, M. Faustino, J.P. Davim, Hard turning: AISI 4340 high strength low alloy steel and AISI D2 cold work tool steel, Journal of Materials Processing Technology 169 (2005) 388-395.
[16] M. Liu, J.-I. Takagi, A. Tsukuda, Effect of tool nose radius and tool wear on residual stress distribution in hard turning of bearing steel, Journal of Materials Processing Technology 150 (2004) 234-241.
[17] I. Mankova, G. Markova, Evaluation of surface microgeometry when grinding and finish turning of hardened steel, Proceedings of the 3rd International Congress of Precision Machining ICPM'2005, Vienna, 2005, 231-237.
[18] D. Novovic, R.C. Dewes, D.K. Aspinwall, W. Voice, P. Bowen, The effect of machined topography and integrity on fatigue life, International Journal of Machine Tools and Manufacture 44 (2004) 125-134.
[19] J. Rech, A. Moisan, Surface integrity in finish hard turning of case-hardened steels, International Journal of Machine Tools and Manufacture 43 (2003) 543-550.
[20] H.K. Tönshoff, C. Arendt, R. Ben Amor, Cutting of hardened steel, CIRP Annals 49 (2000) 547-566.
[21] H.K. Tönshoff, T. Friemuth, C. Marzenell, Properties of honed gears during lifetime, CIRP Annals 49 (2000) 431-434.
[22] J.M. Zhou, M. Andersson, J.E. Stahl, Identification of cutting errors in precision hard turning process, Journal of Materials Processing Technology 153-154 (2004) 746-750.
[23] New developments in hard part machining, 2002 (www.SandvikCoromant.com).
[24] MICROFINISH® Machining of transmission and engine parts, ball and roller bearings, thrusts and sealing faces (www.thielenhaus.us).
[25] X-Ray Diffraction Systems (www.emsl.pnl.gov/capabs).